Real gas effects on ammonia-oxygen laminar flame speed

Fernando Veiga-López[1], Zifeng Weng[2], Rémy Mével[3], Gaofeng Wang[3]
[1]Aerolab, Instituto de Física e Ciencias Aeroespaciais (IFCAE), Universidade de Vigo, Ourense, Galicia, España
[2]School of Vehicle and Mobility, Tsinghua University, Beijing, China
[3]School of Aeronautics and Astronautics, Zhejiang University, Hangzhou, China

1 Introduction

The achievement of carbon neutrality in the coming decades is a major goal of many countries, which implies replacing fossil fuels with clean and renewable energy sources, such as wind and sun light. However, the intrinsic discontinuous characteristic of renewable energy production is an important drawback for industrial and domestic activities, which requires developing energy storage strategies to supply on an almost-continuous demand. In this framework, ammonia is a promising chemical storage candidate [1] with still unknown combustion features that are currently being addressed.

In this regard, the laminar flame speed (LFS) is an important global combustion parameter used to characterize flammable mixtures [2]. The literature for NH_3 and its blends with other fuels, i.e., H_2 [3] and CH_4 [4] is extensive and has grown exponentially in recent years, both experimental and numerical, covering a wide range of conditions [5]. The common missing piece is that, although NH_3 is known to have a strong non-ideal behavior [6], herein referred to as real gas (RG) effect, this aspect has been largely ignored in previous works on LFS. Only a limited number of studies on the effects of RG on LFS exist, all of them focusing on other fuels such as hydrogen or methane [7, 8]. Despite these, among others, relevant studies, it remains unclear under which conditions RG effects should be taken into account for ammonia-based flames. Therefore, aiming to fill this gap, our goal is to evaluate the extent of RG effects on the LFS of ammonia-oxygen (NH_3-O_2) mixtures.

2 Computational methodology and theoretical modeling

Given a one-dimensional, constant pressure configuration, the equations of conservation for mass, species mass fractions, and energy for an inviscid fluid in a gravity-less environment are [9]

$$\frac{D\rho}{Dt} = -\rho\frac{\partial u}{\partial x}, \tag{1a}$$

$$\rho\frac{DY_i}{Dt} = \dot{\omega}_i - \frac{\partial \rho Y_i u_{d,i}}{\partial x}, \tag{1b}$$

$$\rho c_p \frac{DT}{Dt} = -\sum_{i=1}^{N} \bar{h}_i \dot{\omega}_i + \frac{\partial}{\partial x}(\lambda\frac{\partial T}{\partial x}) - \sum_{i=1}^{N} \rho Y_i u_{d,i} \bar{c}_{p,i} \frac{\partial T}{\partial x}. \tag{1c}$$

The momentum equation is not included due to the low-Mach assumption. The novelty is that the Redlich-Known (RK) equation of state (EoS) was used to account for RG effects on the EoS and the

mixture thermodynamic properties:

$$P = \frac{\rho RT}{1-\rho b} - \frac{a\rho^2}{1+\rho b}. \tag{2}$$

P: pressure; R: specific gas constant; a: intermolecular attraction term; and b: co-volume. Expressions of a, b, mixing rules and the thermodynamic functions can be found in [7]. The RG effects on the mass action law are included using the approach of Giovangigli et al. [10],

$$\dot{r}_j = k_{f,j}\prod_i \left(\frac{X_i\phi_i P}{RT}\right)^{\nu'_{i,j}} - k_{r,j}\prod_i \left(\frac{X_i\phi_i P}{RT}\right)^{\nu''_{i,j}}. \tag{3}$$

X_i: mole fraction; ϕ_i: fugacity coefficient; $k_{f,j}$/$k_{r,j}$: forward/backward reaction rate constants; $\nu'_{i,j}$/$\nu''_{i,j}$: stoichiometric coefficients of the i^{th} species as reactant/products, and j: j^{th} reaction. The reaction rate $k_{f,j}$ follows the Arrhenius form, while $k_{r,j}$ is evaluated with $k_{f,j}/K_{c,j}$ where $K_{c,j}$ is the equilibrium constant. The expressions of $K_{c,j}$ and ϕ_i are in [7]. Additionally, transport properties are corrected for high-pressure conditions. The model of Chung et al. [11], modified by Gopal et al. [12], is used to calculate the thermal conductivity. The binary diffusion coefficients were obtained using the Takahashi's model [13]. The mixture-averaged transport model is used.

Calculations for the RK cases were performed using *FreeFlameRK*, a modified freely-propagating flame solver, implemented in Cantera 2.4 [14], see details in [7]. Calculations for the ideal (IG) case were performed with the default flame solver of Cantera, i.e., *FreeFlame*, in which the IG EoS and thermodynamics are used. The steady planar flame solutions were obtained in 5 cm domain which contained more than 2000 points to ensure grid-independence.

Two recent reaction mechanisms are used: (i) Zhang et al. [15], 264 reactions and 38 species; and (ii) Stagni et al. [16], 203 reactions and 31 species. Both mechanisms were extensively validated and utilized in the recent ammonia LFS study of Hamadi et al. [17].

3 Results and discussion

NH_3-O_2 mixtures with equivalence ratios $\Phi = 0.5$, 1, and 2 are considered. To cover a wide range of conditions, calculations are performed for initial temperatures and pressures in the close vicinity of the saturation curve of NH_3 between its triple point ($T_t = 195.5$ K, $P_t = 6.09$ kPa) and its critical point ($T_c = 405.2$ K, $P_c = 11.36$ MPa) [18]. The table included in Fig. 1 provides the initial thermodynamic states, and the compressibility factors (Z) of the mixtures.

3.1 Laminar flame speed and burning flux

Figure 1 shows the LFS of NH_3-O_2 mixtures calculated with the IG and RK models and $\Phi = 2$. The two reaction mechanisms provide similar overall qualitative and quantitative trends, although the predicted LFS can differ significantly under some conditions (note shown here for conciseness), in line with Hamadi et al. [17]. For the shown cases, LFS calculated with the IG model continuously increases as pressure and temperature of the mixtures are increased. On the contrary, including the RK model makes LFS to increase until point 6, then it decreases. The difference between the predictions of the IG and RK models reaches up to 29% with the maximum difference obtained for point 16 at $T = 410$ K and $P = 11.34$ MPa.

#	T (K)	P (MPa)	Z
1	215	0.0177	0.998-0.999
2	225	0.0338	0.996-0.998
3	235	0.0604	0.994-0.997
4	245	0.1022	0.991-0.995
5	255	0.1649	0.987-0.993
6	275	0.3811	0.976-0.987
7	295	0.7774	0.960-0.978
8	305	1.062	0.950-0.973
9	315	1.424	0.938-0.967
10	325	1.873	0.925-0.961
11	335	2.421	0.910-0.954
12	355	3.866	0.877-0.940
13	375	5.878	0.839-0.926
14	395	8.605	0.799-0.913
15	405	10.31	0.778-0.908
16	410	11.34	0.767-0.905

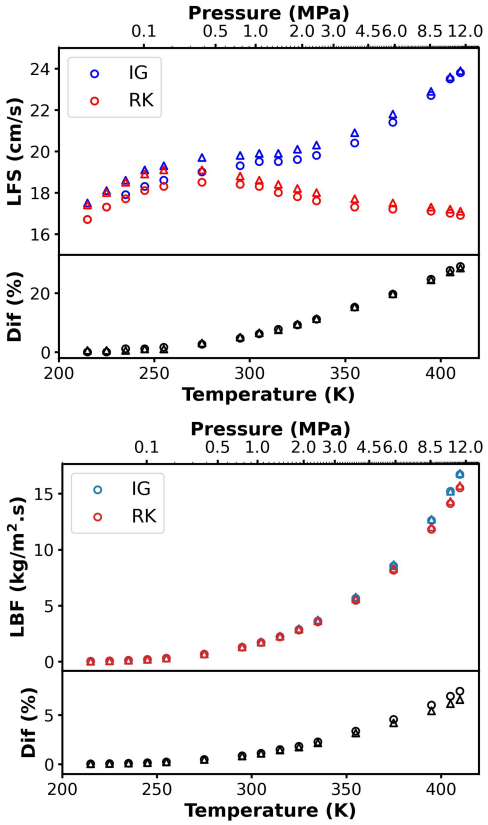

Figure 1: Table includes temperature, pressure, compressibility factor (Z). At each condition, a range of Z, increasing with Φ, is given. *Top*-LFS and *Bottom*-LBF predicted by IG and RK models for NH_3-O_2 with Φ =2. Triangles: [15]; circles: [16].

According to [19, 20], the laminar burning flux (LBF), i.e., the LFS multiplied by the fresh gas density, is the actual "eigenvalue" of one-dimensional planar flames, indicating that LBF should coincide regardless of the gas model used. The LBF for the different ammonia-based mixtures is presented in Fig. 1 as well. Unlike LFS, which demonstrates complex variations as pressure and temperature are varied, LBF shows a continuous increase. In addition, LBF calculated with the IG and RK models are not exactly the same, consistent with the results of [7] on the RG effects on LFS of sCO_2-diluted syngas- and methane-based mixtures. While the difference in LBF is significantly lower than for the LFS, it remains above 5% for rich NH_3-O_2 under high-pressure conditions.

3.2 Analysis of the real gas effects

To further explore the origin of the differences between the IG and RK models and following the lead of previous studies [7, 10, 21], the contribution of several parts of the RK model can be more clearly identified by progressively incorporating new feature to the initial IG model. To clarify the notation:

- Model 1 (M1 or IG): IG
- Model 2 (M2): + RK EoS and thermodynamics
- Model 3 (M3): + high-pressure transport
- Model 4 (M4 or RK): + modified kinetics (Eq. 3)

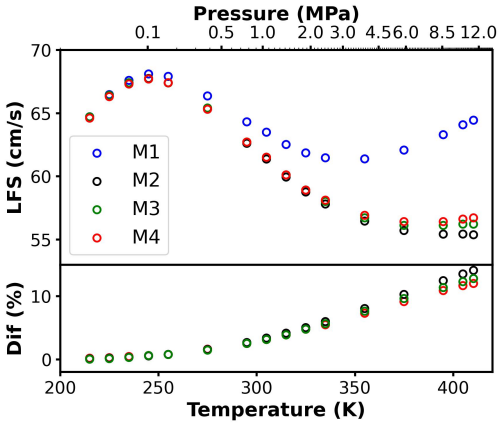

Figure 2: LFS for a NH_3-O_2 mixture with $\Phi = 0.5$. Chemistry from [16] and different gas models.

Figure 2 shows the LFS for the lean NH_3-O_2 mixture obtained when considering these different sets of assumptions. The said equivalence ratios were computed and discussed, but not included for conciseness. For all compositions and conditions investigated, no modification of the reported qualitative trends is observed from M2 to M4. Nevertheless, while the LFS obtained with M2 to M4 are close to each other, they do not exactly match quantitatively. For instance, for the NH_3-O_2 mixture with $\Phi = 0.5$ and the conditions of point 16, the difference between M1 and M4 is of 12%; the one between M1 and M2 is of 14.1%, which represents a relative increase of 17%.

Let's recall the expression of the LFS derived by Mallard and Le Chatelier, and by Zeldovich, Frank-Kamenetskii and Semenov [22],

$$\text{LFS} \propto \sqrt{\frac{\lambda}{\rho_u c_p} \times \frac{d\psi}{dt}} = \sqrt{\alpha \times \dot{\omega}}. \tag{4}$$

α: thermal conductivity; ψ: progress variable; and $\dot{\omega}$: reaction rate.

Changing from M1 to M2 induces a change of α through the modification of the fresh gas density and of the heat capacity, see Fig. 3. Both quantities are largely increased by the change in the EoS and thermodynamics functions, which leads to a significantly higher LFS in a high-pressure IG.

In addition, moving from M1 to M2 affects the $\dot{\omega}$ through the modification of temperature, of the enthalpy of reaction, and of the Gibbs free energy. The flame temperature depends on the equilibrium composition which is modified by the RG effects. These aspects are illustrated in Fig. 3. Depending on Φ, significantly less or more ammonia is consumed when considering RG effects, and in most conditions, the amount of N_yO_x formed is lower when including RG EoS and thermodynamics. These observations indicate that RG effects should be accounted for when evaluating the production of pollutants formed during high-pressure combustion of ammonia-based mixtures.

4 Conclusion

The influence of including real fluid modeling was investigated for NH_3-O_2 LFS calculations along the vapor saturation curve of ammonia. Results show a strong influence of RG effects on the computed LFS of the tested mixtures. Qualitatively, the IG model yields a continuous increase of the LFS with pressure

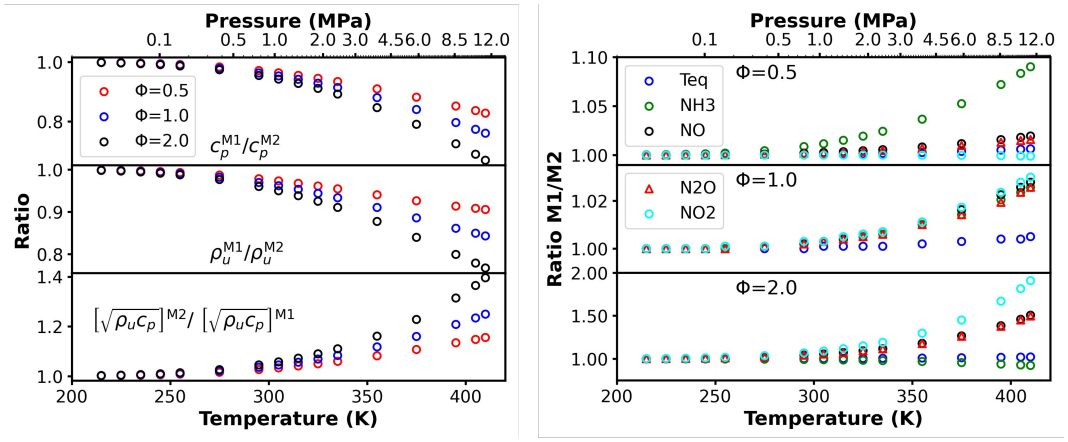

Figure 3: *Left* - RG impact on c_p and ρ_u. *Right* - Constant pressure equilibrium temperature and mole fraction ratios. NH_3-O_2 mixtures using the chemistry from [16].

and temperature, while including RG effects results in a decrease of the LFS for $P > 1.062$ MPa and $T > 275$ K. Quantitatively, the largest discrepancy is found for the highest combination of pressure and temperature, up to 29 % for a NH_3-O_2 mixture with Φ=2. Progressively adding real gas effects, i.e., EoS and thermodynamics, transport, and chemical kinetics, shows that the main aspects responsible for the change of LFS are the real gas EoS and thermodynamics, while high-pressure transport models and kinetics are of second-order importance. In light of the results, RG effects should be included when modeling NH_3 combustion in future analyses.

References

[1] A. Valera-Medina, H. Xiao, M. Owen-Jones, W. David, and P. Bowen, "Ammonia for power," *Prog. Energy Combust. Sci.*, vol. 69, pp. 63–102, 2018.

[2] D. Smooke, J. Miller, and R. Kee, "Determination of adiabatic flame speeds by boundary value methods," *Combust. Sci. Technol.*, vol. 34, no. 1-6, pp. 79–90, 1983.

[3] K. Shrestha, C. Lhuillier, A. Alves Barbosa, P. Brequigny, F. Contino, C. Mounaim-Rousselle, L. Seidel, and F. Mauss, "An experimental and modeling study of ammonia with enriched oxygen content and ammonia/hydrogen laminar flame speed at elevated pressure and temperature," *Proc. Combust. Inst.*, vol. 38, pp. 2163–2174, 2021.

[4] R. Rocha, S. Zhong, L. Xu, X. Bai, M. Costa, X. Cai, H. Kim, C. Brackmann, Z. Li, and M. Alden, "Structure and laminar flame speed of an ammonia/methane/air premixed flame under varying pressure and equivalence ratio," *Energy Fuels*, vol. 35, no. 9, pp. 7179–7192, 2021.

[5] M. Figueroa-Labastida, L. Zheng, J. Streicher, and R. Hanson, "Ammonia/hydrogen laminar flame speed measurements at elevated temperatures," *Int. J. Hydrog. Energy*, vol. 63, pp. 1137–1146, 2024.

[6] Z. Weng, R. Mével, and N. Chaumeix, "Detonation in ammonia-oxygen and ammonia-nitrous oxide mixtures," *Combust. Flame*, vol. 251, p. 112680, 2023.

[7] Y. Zhang, Z. Weng, and R. Mével, "Laminar flame speeds of supercritical CO2 diluted oxy-syngas and oxy-methane flames under direct-fired power cycle relevant conditions," *Combust. Flame*, vol. 266, p. 113526, 2024.

[8] Z. Weng, Y. Zhang, B. Maxwell, and R. Mével, "The effect of finite molecular volume on the propagation of unsteady spherical flame front," *Combust. Flame*, vol. 263, p. 113404, 2024.

[9] C. K. Law, *Combustion Physics*. Cambridge University Press, 2010.

[10] V. Giovangigli, L. Matuszewski, and Francis Dupoirieux, "Detailed modeling of planar transcritical H_2-O_2-N_2 flames," *Combust. Theory Model.*, vol. 15, no. 2, pp. 141–182, 2011.

[11] T. Chung, M. Ajlan, L. Lee, and K. Starling, "Generalized multiparameter correlation for nonpolar and polar fluid transport properties," *Ind. Eng. Chem. Res.*, vol. 27, no. 4, pp. 671–679, 1988.

[12] A. Gopal, P. Volpiani, S. Yellapantula, and J. Larsson, "Computational investigation of real fluid effects in cryogenic laminar premixed CH_4-O_2 flames," *J. Supercrit. Fluids*, vol. 168, p. 105045, 2021.

[13] S. Takahashi, "Preparation of a generalized chart for the diffusion coefficients of gases at high pressures," *J. Chem. Eng. Jpn.*, vol. 7, no. 6, pp. 417–420, 1975.

[14] D. G. Goodwin, R. L. Speth, H. K. Moffat, and B. W. Weber, *Cantera: An object-oriented software toolkit for chemical kinetics, thermodynamics, and transport processes*, 2018.

[15] X. Zhang, S. Moosakutty, R. Rajan, M. Younes, and S. Sarathy, "Combustion chemistry of ammonia/hydrogen mixtures: Jet-stirred reactor measurements and comprehensive kinetic modeling," *Combust. Flame*, vol. 234, p. 111653, 2021.

[16] A. Stagni, S. Arunthanayothin, M. Dehue, O. Herbinet, F. Battin-Leclerc, P. Brequigny, C. Mounaim-Rousselle, and T. Faravelli, "Low- and intermediate-temperature ammonia/hydrogen oxidation in a flow reactor: Experiments and a wide-range kinetic modeling," *Chem. Eng. J.*, vol. 471, p. 144577, 2023.

[17] A. Hamadi, N. Obrecht, C. Callu, A. Stagni, T. Faravelli, A. Comandini, and N. Chaumeix, "Experimental and modeling investigation of the laminar flame speeds for ammonia with various oxygen and diluent mixtures," *Proc. Combust. Inst.*, vol. 40, p. 105387, 2024.

[18] L. Glasser, "Equations of state and phase diagrams of ammonia," *J. Chem. Educ.*, vol. 86, no. 12, p. 1457, 2009.

[19] C. K. Law, *Combustion Physics*. Cambridge University Press, 2006.

[20] W. Liang and C. Law, "Theory of supercritical flames with real-fluid equations of state," *Combust. Theory Model.*, vol. 25, no. 6, pp. 1002–1018, 2021.

[21] W. Liang, W. Li, and C. Law, "Laminar flame propagation in supercritical hydrogen/air and methane/air mixtures," *Proc. Combust. Inst.*, vol. 37, pp. 1733–1739, 2019.

[22] I. Glassman, R. Yetter, and N. Glumac, *Combustion*, 5th ed. Academic Press, 2014.